distributed to the rest of the sample which increases δd and P_t for the rest of the SDLs, providing the basic mechanism for the cascade which finally moves out from the center of the sample as a well-defined front of helixing SDLs. The shape of the tail of the relaxation is determined by the drop elliptical shape, with slower relaxations when the range of ρ determining the drop boundary varies over a larger range. Although the precise value of $\delta d/\delta t$ at any point in the step depends on the exact size and shape of the LC sample, the qualitative features exhibited are relatively constant.

To model the multiple layer events shown in Fig. 1C, we assumed that some fraction (~10%) of the SDLs undergo multiple nucleations, an assumption which also tends to improve the qualitative correspondence of the single-step simulations to the experimental data. When one smectic A layer has been removed from nearly the entire sample, the dilation in the center, due to the multiply nucleated SDLs, is slightly greater than what it was initially, and the process quickly begins again. The multiply nucleated SDLs will not ordinarily undergo a second instability because the dilation in this area was already relieved by more than one layer, greatly reducing the nucleation probability. Thus, because of the lower average force and therefore dilation at the time of each second helical instability, this second step is significantly slower.

We have studied phase slippage events in the layering order parameter $\phi(\mathbf{r})$ of a smectic A in a thin spherical wedge. At temperatures well below the nematic–smectic A phase transition, a screw dislocation–mediated process appears at stresses below the threshold for unpinning of the edge dislocations present in the wedge geometry. The data indicate a threshold depending principally on net order parameter phase change (not strain or stress). In the spherical wedge, a weak residual dependence on stress produces an instability of screw dislocation helixing beginning in the cell center, where the stress is highest, and proceeding with an avalanche-like front to the thicker part of the wedge.

REFERENCES AND NOTES

1. P. G. deGennes and J. Prost, *The Physics of Liquid Crystals* (Clarendon, Oxford, ed. 2, 1993); B. S. Chandrasekhar, *Liquid Crystals* (Cambridge Univ. Press, Cambridge, ed. 2, 1993).
2. R. G. Horn, J. N. Israelachvili, E. Perez, *J. Phys. (Paris)* **42**, 39 (1981).
3. P. Kékicheff and H. K. Christenson, *Phys. Rev. Lett.* **63**, 2823 (1989).
4. P. Richetti *et al.*, *Nature* **346**, 252 (1990).
5. J. N. Israelachvili, *Intermolecular & Surface Forces* (Academic Press, London, 1992).
6. P. G. deGennes, *Solid. State Commun.* **10**, 753 (1972).
7. M. Kléman, *Points, Lines, and Walls* (Wiley, New York, 1983).
8. W. I. Glaberson, W. W. Johnson, R. M. Ostermeir, *Phys. Rev. Lett.* **33**, 1197 (1974).
9. J. R. Clem, *ibid.* **38**, 1427 (1977).
10. L. Bourdon, M. Kléman, L. Lejcek, D. Taupin, *J. Phys. (Paris)* **42**, 261 (1981).
11. P. Oswald and M. Kléman, *ibid.* **45**, L319 (1984).
12. P. P. Karat and N. V. Madhusudana, *Mol. Cryst. Liq. Cryst.* **36**, 51 (1976).
13. R. Herke, N. A. Clark, M. A. Handschy, unpublished results; R. Herke, thesis, University of Colorado (1993).
14. D. Davidov *et al.*, *Phys. Rev. B* **19**, 1657 (1979).
15. G. B. Kasting *et al.*, *J. Phys. (Paris)* **41**, 879 (1980); J. Thoen *et al.*, *Phys. Rev. A* **26**, 2886 (1982).
16. M. R. Fisch *et al.*, *Phys. Rev. A* **29**, 2741 (1984); M. Benzekri *et al.*, *Phys. Rev. Lett.* **68**, 2480 (1992).
17. N. A. Clark, *Phys. Rev. A* **14**, 1551 (1976).
18. R. Ribotta and G. Durand, *J. Phys. (Paris)* **38**, 179 (1977); R. Bartolino and G. Durand, *Phys. Rev. Lett.* **39**, 1346 (1977).
19. R. A. Herke, N. A. Clark, M. A. Handschy, data not shown.
20. F. R. N. Nabarro, *Theory of Crystal Dislocations* (Dover, New York, 1967).
21. M. Kléman, *J. Phys. (Paris)* **35**, 595 (1974).

22. This work supported by NSF Solid State Chemistry Grant DMR 92-23729.

13 July 1994; accepted 21 November 1994

Imaging with Intermolecular Multiple-Quantum Coherences in Solution Nuclear Magnetic Resonance

Wolfgang Richter, Sanghyuk Lee, Warren S. Warren,* Qiuhong He

A magnetic resonance imaging technique based on intermolecular multiple-quantum coherences in solution (the correlated spectroscopy revamped by asymmetric *z* gradient echo detection or CRAZED experiment) is described here. Correlations between spins in different molecules were detected by magnetic-field gradient pulses. In order for a correlation to yield an observable signal, the separation between the two spins must be within a narrow band that depends on the area of the gradient pulses. The separation can be tuned from less than 10 micrometers to more than 1 millimeter, a convenient range for many applications.

A variety of nuclear magnetic resonance (NMR) methods have proven useful for extracting structural information. For example, the nuclear Overhauser effect (NOE) (*1*) can be used to determine if two spins are within approximately 5 Å and is crucial for the determination of macromolecular structure. On a much larger scale (millimeters), the internal structure of a sample can be conveniently mapped by magnetic resonance imaging (MRI) (*2*, *3*). The spatial resolution in MRI arises from gradient pulses, which cause spins to evolve at different frequencies in different sample positions; increasing the gradient strength improves the spatial resolution. However, the most important resolution limitation in three-dimensional imaging is not the strength of the gradient pulse. Improving spatial resolution by a factor of 2 decreases the number of spins in each voxel by a factor of 8, and eventually sensitivity considerations dominate. Thus, in practice, imaging with 10-μm resolution is quite challenging.

Here, we show direct experimental evidence of the spatial selectivity of the CRAZED experiment with a set of phantoms. This experiment (Fig. 1) is a conventional correlated spectroscopy (COSY) experiment, modified with an *n*-quantum gradient filter at the second pulse. Our results verify the theoretical model presented by Warren and co-workers (*4*, *5*), which predicted that it should be possible to observe cross peaks between separated samples, but only if the separation is smaller than the pitch of the magnetization helix generated by the gradient pulses. Thus, changing the gradient pulse strength couples or decouples the separated samples. We also discuss the possible application of this approach as an imaging technique.

According to the prevailing theory (*1*, *6*), the CRAZED pulse sequence cannot generate any observable magnetization; the first pulse could merely produce single-quantum coherences, I_x, which would be dephased by the gradient filter unless $n = 1$. However, application of this pulse sequence (with $n = 2$, for example) to a concentrated sample led to observable double-quantum transitions in the indirectly detected dimension (F_1) and single-quantum transitions in the directly detected dimension (F_2). The conclusion was that double-quantum, two-spin coherences must be present after the first pulse in order to evolve in time t_1, and

W. Richter, S. Lee, W. S. Warren, Department of Chemistry, Princeton University, Princeton, NJ 08544, USA. Q. He, Department of Radiology, NMR Research Division, Johns Hopkins University School of Medicine, Baltimore, MD 21205, USA.

*To whom correspondence should be addressed.

that they were transformed into single-quantum, single-spin coherences afterward.

We found it necessary to make two modifications to the conventional density matrix description of solution NMR in order to understand these results (5). First, the assumption that all dipolar couplings between spins can be ignored (7) had to be modified. The dipole-dipole coupling between spins i and j is proportional to $(3\cos^2\theta_{ij} - 1)/r_{ij}^3$, where θ_{ij} is the angle between the internuclear vector and the applied magnetic field and r_{ij} is the internuclear distance. For small values of r_{ij}, θ_{ij} takes all possible values owing to diffusion and the dipolar coupling is averaged away. However, this averaging cannot occur for spins separated by more than the distance molecules diffuse on an NMR time scale ($\approx$10 μm for small molecules). The retained individual couplings are very small, but the total number of spins is very large. If the spatial distribution is made nonuniform (by gradient pulses or even by edge effects), dipolar effects can reappear; the magnitude of this dipolar field is approximately $\gamma\mu_0 M_0$ (where γ is the gyromagnetic ratio, μ_0 is the vacuum permeability, and M_0 is the equilibrium magnetization), which for water at room temperature in a 600-MHz spectrometer is $\approx$14 rad $\cdot$ s^{-1}.

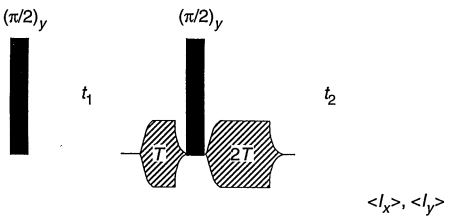

Fig. 1. The CRAZED pulse sequence for $n = 2$. The area of the second gradient pulse is always twice that of the first one; in our experiment, the two gradient pulses have equal duration but different amplitudes. I_x and I_y are the observable magnetization in the x and y directions, respectively.

One way to handle this effect is to modify the Bloch equations by a mean field approximation [the "dipolar demagnetizing field" $\mathbf{B}_d(\mathbf{r})$ (8–13)], which replaces individual spins with the local average magnetization; at least for two-pulse sequences, this approach gives results that agree with experimental values. However, the modified Bloch equations generate nonlinear equations of motion (thus, the conventional propagator-based picture of spin evolution fails completely), and in any event a density matrix picture is more appropriate for molecules with internal structure. The exact density matrix at thermal equilibrium

$$\rho_{eq} \propto \exp(-\beta\hbar\,\omega_o \sum_i^N I_{zi}) \qquad (1)$$

where $\beta = 1/kT$, k is the Boltzmann constant, $\hbar$ is Planck's constant, and ω_0 is the nuclear resonance frequency, is generally expanded in a Taylor series up to the term linear in the Hamiltonian only [the "high-temperature (HT) approximation"]

$$\rho_{HT} \propto (1 - \beta\hbar\,\omega_o \sum_i^N I_{zi}) \qquad (2)$$

Most experiments can be described properly in this limit, but a straightforward analysis reveals that this approximation is extremely dangerous. For example, if the Taylor expansion truly neglected only small terms, the normalization constants for ρ_{eq} and ρ_{HT} would be expected to be quite similar. Instead, for a sample with 10^{22} spins in a 600-MHz spectrometer, the normalization constants differ by a factor of $e^{-5 \times 10^{13}}$. In addition, the most populated states in ρ_{eq} are those with nearly the equilibrium magnetization, which under these conditions has 10^{18} more spins aligned parallel to the field; the most populated states in ρ_{HT} have nearly the same number of spins up and down. Thus, whenever the bulk magnetization matters, the HT approximation is expected to be inadequate.

Expansion of the density matrix beyond the linear term yields the observed two-spin and multispin correlations. They are usually not detected in COSY experiments because there is no mechanism that transforms them into observable (single-quantum) magnetization. In the CRAZED experiment, however, the gradient pulses create a magnetically anisotropic environment and the long-range dipolar interactions generate observable magnetization. The strength of the correlation signal depends on the distance between the two spins and on the pitch of the helix that the gradient pulses generate (5). Warren *et al.* (5) showed the signal arising at spin 1 by the action of spin 2 to be

$$\frac{\text{CRAZED signal}}{\text{COSY diagonal peak}} = \frac{3}{32\pi}\frac{t_2}{\tau_d}(r_1 - r_2)^{-3} \times (3\cos^2\theta - 1)\cos[\gamma G T(z_2 - z_1)] \qquad (3)$$

where τ_d is the dipolar demagnetizing time, θ is the angle between the internuclear vector and the z axis, T is the gradient pulse length, and the gradient G is oriented along the z direction here. The total signal is the sum of this function over all spin pairs, which, for a macroscopic sample, can be replaced by an integral. The pitch of the magnetization (single-quantum) helix is $2\pi/2\gamma GT = \pi/\gamma GT$ because the intensity of the second gradient pulse is 2G.

For a hypothetical sample where each spin is at the center of a sphere with a radius that is large as compared to the helix pitch, the bulk of the signal comes from spins separated by about one helix pitch (5). This

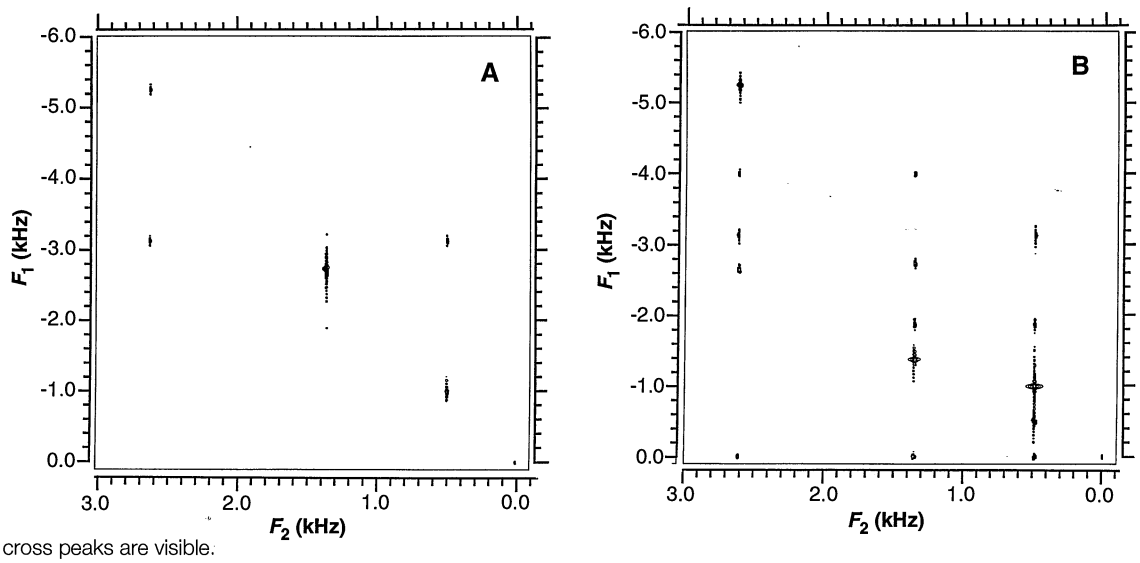

Fig. 2. CRAZED spectra for a sample consisting of nested cylinders. In the outside cylinder are benzene (B) (F_{2B} = 2620 Hz), acetone (A) (F_{2A} = 493 Hz), and deuterated acetone. In the inside cylinders is water (W) (F_{2W} = 1358 Hz). Cross peaks in F_1 are expected at the negative of the sum of the F_2 frequencies: $F_{1(A+A)}$ = −986 Hz; $F_{1(B+B)}$ = −5240 Hz; $F_{1(W+W)}$ = −2716 Hz; $F_{1(A+B)}$ = −3113 Hz; $F_{1(B+W)}$ = −3978 Hz; and $F_{1(A+W)}$ = −1851 Hz. (**A**) Strong gradient, short helix pitch: only cross peaks for molecules within one tube are visible. (**B**) Weak gradient, long helix pitch: all possible cross peaks are visible.

suggested that the magnitude of the cross peaks could be used for imaging. Here, we integrated Eq. 3 for a variety of different sample geometries and for various gradient strengths (Table 1). The fourth column of Table 1 shows the effects of a cylindrical sample; the height of the cylinder is chosen to be 15 mm, and its radius 2.1 mm—a typical "5 mm" (outside diameter) NMR tube. The duration of the (sine-bell–shaped) gradient pulses is 1 ms, and the maximum strength of the first gradient pulse is varied from 1.49×10^{-2} to 1.18×10^{-1} T m^{-1}. The last row in Table 1 corresponds to an infinitely large gradient (which makes the sample infinitely large in units of helix pitch), for which the integral can be solved analytically. The strength of the double-quantum signal increases monotonically with the gradient strength to converge at a value of $-8\pi/3$ for an infinitely large sample. This limiting value is the same as for the spherical sample considered by Warren *et al.* (5). The sample shape is of no consequence if the sample is infinitely large.

Equation 3 was also numerically integrated for cross peaks between two nested cylindrical samples. The dimensions of the outer tube were the same as before, and the inner tube had an outer diameter of 1 mm and a wall thickness of 0.1 mm, and it touched the wall of the outer tube. The results are also given in Table 1. In this case, the signal intensity decreases with increasing gradient strength; in fact, there is virtually no signal if the helix pitch is less than several times the wall thickness. This is expected; as noted earlier, the bulk of the signal comes from a distance of approximately one helix pitch.

We performed a series of double-quantum CRAZED experiments with varying gradient amplitudes on a GE 9.4 T Omega CSI NMR spectrometer with shielded gradients. The sample was a regular 5-mm NMR tube containing a mixture of equal volumes of benzene, acetone, and deuterated acetone. Inside the tube were three capillary tubes containing water; these tubes touched the wall of the outer tube and each other. The sample dimensions and gradient strengths were the same as in the calculation above.

Two of the spectra are graphed in Fig. 2. Figure 2A shows the spectrum for $G_{max} = 1.18 \times 10^{-1}$ T m^{-1}. The helix pitch is $\pi/\gamma GT = 0.156$ mm, with $G = G_{max} \times 2/\pi$ for the sine-bell–shaped gradient. All three homomolecular double-quantum peaks are visible, as well as a heteromolecular double-quantum peak between benzene and acetone. There are no cross peaks between the tubes (between water and either acetone or benzene). Figure 2B shows the spectrum for $G = 1.49 \times 10^{-2}$ T m^{-1}, with a helix pitch of 1.24 mm. Unlike Fig. 2A, Fig. 2B shows additional cross peaks between water and benzene and water and acetone. Also visible are single-quantum peaks, caused by imperfect suppression; as there are only a few turns of the magnetization helix across the whole sample, averaging of the magnetization is incomplete.

Figure 3 graphs the experimental and calculated double-quantum peak intensities. All values are normalized to the most intense water double-quantum peak. As predicted, varying the gradient strength selects a minimum interaction distance (the water double-quantum peak vanishes when the helix pitch is large compared to the dimensions of the capillary tube) as well as a maximum interaction distance (for short helix pitches, there is no signal across the glass wall).

The direction of the interaction can be selected as well. Numerical simulations for concentric tubes show that the intensity of the double-quantum peaks between different molecules within the same sample tube follows the characteristic dependence on the angle between the magnetic field and the gradient [$\Delta = (3\cos^2\theta - 1)/2$] and that the magic-angle gradient quenches the intermolecular double-quantum correlations (5). However, the cross peaks between the tubes vanish for an x gradient, not for a magic-angle gradient. Experiments with an x gradient confirm the numerical simulations. This shows that the cross-peak intensity is a sensitive function of the spin distribution.

Increasing the gradient strength increases the resolution of the experiment, until molecular diffusion effectively blurs out the magnetization anisotropy the gradient pulses create. This suggests a practical resolution limit of a few micrometers for a small molecule such as water. Aside from that, increasing resolution does not decrease sensitivity because the signal comes from the entire sample and depends only on the local magnetization density at the two spots. Although decreasing the distance of the interaction decreases the interacting volume, the interaction strength rises by the same factor because it is based on dipolar couplings.

The CRAZED experiment might be a very useful probe for large-scale molecular interactions or material structure. It complements the study of diffusion or flow by pulsed gradient spin echoes (PGSEs) (*14, 15*). In the PGSE method, the echo intensity is measured in **k** space (where k is proportional to the area of the gradient pulse). Fourier transform of the signal into real space yields a displacement distribution function; in our case, we can measure diffusion or flow of coherences involving separated spins. Similarly, the distance information obtained in the CRAZED experiment can yield a Patterson-type spatial spin-pair correlation function. For example, the concentration of water around a protein as a function of distance can be determined

Table 1. Calculated signal intensities.

G_{max} (10^{-2} T × m^{-1})	Helix pitch (mm)	γGT (mm^{-1}) ($G = G_{max} \times 2/\pi$)	Signal for a single cylinder, per unit volume (z gradient)	Signal between two nested cylinders per unit outer volume (z gradient)
1.49	1.24	2.54	0.025	−0.172
1.98	0.932	3.37	−1.09	−0.147
2.97	0.621	5.06	−2.79	−0.103
5.95	0.311	10.1	−5.22	−0.038
11.8	0.156	20.1	−6.65	−0.008
∞	0	∞	−8.38	0

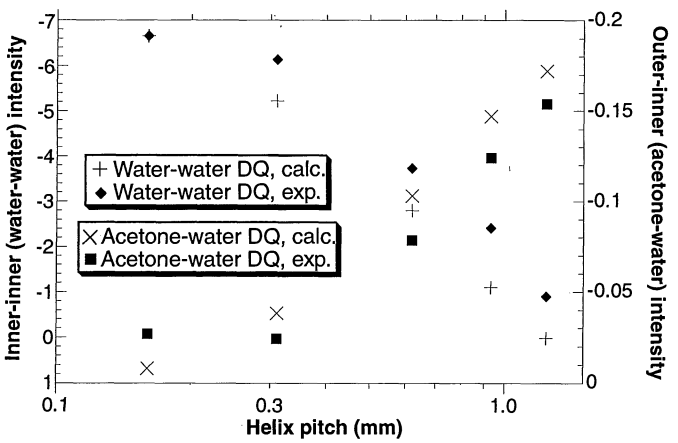

Fig. 3. Calculated and experimental double-quantum (DQ) cross-peak intensities as functions of helix pitch.

by this method; this method should be sensitive to cell structure, providing an alternative to conventional MRI (which uses relaxation-weighted spin density). Experiments of this type can be performed with any NMR spectrometer if variable linear magnetic-field gradients are available. Although a large spin concentration is required to generate the dipolar demagnetizing field, this condition is always fulfilled in aqueous solution.

REFERENCES AND NOTES

1. See, for example, R. R. Ernst, G. Bodenhausen, A. Wokaun, *Principles of Nuclear Magnetic Resonance in One and Two Dimensions* (Clarendon, Oxford, 1987).
2. S. C. Bushong, *Magnetic Resonance Imaging: Physical and Biological Principles* (Mosby, St. Louis, 1988).
3. D. W. Chakeres and P. Schmalbrock, *Fundamentals of Magnetic Resonance Imaging* (Williams & Wilkins, Baltimore, 1992).
4. Q. He, W. Richter, S. Vathyam, W. S. Warren, *J. Chem. Phys.* **98**, 6779 (1993).
5. W. S. Warren, W. Richter, A. Hamilton Andreotti, B. T. Farmer II, *Science* **262**, 2005 (1993).
6. A. Abragam, *The Principles of Nuclear Magnetism* (Clarendon, Oxford, 1961).
7. N. Bloembergen, E. M. Purcell, R. V. Pound, *Phys. Rev.* **73**, 679 (1948).
8. G. Deville, M. Bernier, J. M. Delrieux, *Phys. Rev. B* **19**, 5666 (1979).
9. D. Einzel, G. Eska, Y. Hirayoshi, T. Kopp, P. Wölfle, *Phys. Rev. Lett.* **53**, 2312 (1984).
10. R. Bowtell, R. M. Bowley, P. Glover, *J. Magn. Reson.* **88**, 643 (1990).
11. H. Körber *et al.*, *ibid.* **93**, 589 (1991).
12. A. S. Bedford, R. Bowtell, R. M. Bowley, *ibid.*, p. 516.
13. R. Bowtell, *ibid.* **100**, 1 (1992).
14. P. Callaghan, *Principles of Nuclear Magnetic Resonance Microscopy* (Clarendon, Oxford, 1991).
15. G. C. Chingas, L. Frydman, G. A. Barrall, J. S. Harwood, in *Magnetic Resonance Microscopy*, B. Blümich and W. Kuhn, Eds. (VCH, Weinheim, 1992), pp. 373–393.

16. This work was supported under NIH contract GM35253.

27 July 1994; accepted 16 November 1994

Neutron Reflection Study of Bovine β-Casein Adsorbed on OTS Self-Assembled Monolayers

Giovanna Fragneto, Robert K. Thomas, Adrian R. Rennie,* Jeffrey Penfold

Specular neutron reflection has been used to determine the structure and composition of bovine β-casein adsorbed on a solid surface from an aqueous phosphate-buffered solution at pH 7. The protein was adsorbed on a hydrophobic monolayer self-assembled from deuterated octadecyltrichlorosilane solution on a silicon (111) surface. A two-layer structure formed consisting of one dense layer of thickness 23 ± 1 angstroms and a surface coverage of 1.9 milligrams per square meter adjacent to the surface and an external layer protruding into the solution of thickness 35 ± 1 angstroms and 12 percent protein volume fraction. The structure of the (β-casein) layer is explained in terms of the charge distribution in the protein.

The mechanism of adsorption of proteins at interfaces and the structure and homogeneity of the adsorbed layer are important prerequisites for a full understanding of the role of proteins in the stabilization of foams and emulsions and provide essential information for research in protein chromatography (*1*), biomedical materials (*2*), and cellular adhesion (*3*). There are therefore a large number of studies involving protein adsorption at both solid-liquid interfaces, such as on colloidal particles (*4–7*), on metal surfaces (*8, 9*), on silica surfaces (*10, 11*), and on polymer surfaces (*12*), and at air-liquid interfaces (*13–15*). The adsorption is so sensitive to the nature of the substrate that is it difficult to construct theoretical models, and it is therefore desirable to work with well-defined interfaces.

We have used neutron reflectivity (*16*) to determine the structure of the milk protein β-casein adsorbed on a chemically modified hydrophobic silicon surface. A hydrophobic self-assembled monolayer (SAM), formed on the silicon surface from octadecyltrichlorosilane (OTS) solution, was first characterized and then studied with a monolayer of protein. A hydrophobic surface was chosen because the conformation of proteins is, in most cases, determined by hydrophobic interactions in the nonpolar residues of the peptide chains.

The molecule β-casein is a single-chain protein with a known sequence of 209 residues (*17*) and a molecular mass of ~24,000 daltons. It has a 21-residue amino terminal sequence that contains one-third of the charged residues that the molecule has at pH 7. The remainder of the polypeptide side chains are mostly nonpolar and hydrophobic, and so the molecule is amphiphilic and surface-active. Sedimentation field-flow fractionation and dynamic light scattering of β-casein adsorbed on colloidal polystyrene latices (*5, 6*) indicate that this protein is a flexible molecule with a highly hydrophobic "tail," which may be the site of adsorption to nonpolar surfaces, and a hydrophilic portion that penetrates deeply into the aqueous environment. Prime and Whitesides have studied the adsorption of various proteins on SAMs of ω-functionalized long-chain alkanethiolates on gold (*9*) and found that they are excellent model systems for studying the interactions of proteins with organic surfaces.

We used the specular reflectivity of neutrons, which has recently proved to be a successful technique for studies of solid-liquid interfaces (*18*), to obtain valuable complimentary information on β-casein adsorption at a hydrophobic silicon surface. The experimental details have been given elsewhere (*19*). The technique has been used for the characterization of monolayers formed from OTS on silicon blocks (*20*) and offers several advantages over traditional methods. In a neutron reflection experiment, the specular reflection R is measured as a function of the wave vector transfer κ perpendicular to the reflecting surface, where $\kappa = (4\pi/\lambda)\sin\theta$ (θ is the glancing angle of incidence and λ is the wavelength of the incident neutron beam). The relation of R to the scattering length density across an interface, $\rho(z)$, is given by

$$R(\kappa)=\frac{16\pi^2}{\kappa^2}\,|\,\tilde{\rho}(\kappa)\,|^2 \qquad (1)$$

where $\tilde{\rho}(\kappa)$ is the one-dimensional Fourier transform of $\rho(z)$, that is

$$\tilde{\rho}(\kappa)=\int_{-\infty}^{+\infty}\exp(-i\kappa z)\rho(z)dz \qquad (2)$$

(ρ is a function of the distance z perpendicular to the interface).

In a typical analysis, the measured data are compared with a reflectivity profile calculated according to the optical matrix method (*21*) for different model density profiles. A model consists of a series of layers, each with a scattering length density ρ and thickness t. An additional parameter σ, the interfacial roughness between any two consecutive layers, may also be included in the matrix calculation. By variation of ρ and t for each layer, the calculated profile may be compared with the measured profile until the optimum fit to the data is found. Although any one profile may not provide a unique solution, one can obtain an unambiguous model of the interface by using different isotopic contrasts.

G. Fragneto and R. K. Thomas, Physical Chemistry Laboratory, Oxford University, South Parks Road, Oxford OX1 3QZ, United Kingdom.
A. R. Rennie, Cavendish Laboratory, Cambridge University, Madingley Road, Cambridge CB3 0HE, United Kingdom.
J. Penfold, Rutherford Appleton Laboratory, Chilton, Didcot, Oxon OX11 0QX, United Kingdom.
*To whom correspondence should be addressed.